High-pressure sprayed siRNAs influence the efficiency but not the profile of transitive silencing

Veli Vural Uslu[1*], Athanasios Dalakouras[2], Victor A Steffens[1], Gabi Krczal[1], Michael Wassenegger[1,3*]

[1]AlPlanta-Institute for Plant Research, RLP AgroScience GmbH, Neustadt an der Weinstraße, Germany

[2] Institute of Industrial and Forage Crops, Hellenic Agricultural Organization ELGO-DEMETER, Larissa, Greece

[3]Centre for Organismal Studies Heidelberg, University of Heidelberg, Heidelberg, Germany

*Corresponding author

SUMMARY

In plants, small interfering RNAs (siRNAs) are a quintessential class of RNA interference (RNAi)-inducing molecules produced by the endonucleolytic cleavage of double stranded RNAs (dsRNAs). In order to ensure robust RNAi, siRNAs are amplified through a positive feedback mechanism called transitivity. Transitivity relies on RNA-DIRECTED-RNA POLYMERASE 6 (RDR6)-mediated dsRNA synthesis using siRNA-targeted RNA. The newly synthesized dsRNA is subsequently cleaved into secondary siRNAs by DICER-LIKE (DCL) endonucleases. Just like primary siRNAs, secondary siRNAs are also loaded into ARGONAUTE proteins (AGOs) to form an RNA-induced silencing complex (RISC) reinforcing the cleavage of the target RNA. Although the molecular players underlying transitivity are well established, the mode of action of transitivity remains elusive. In this study, we investigated the influence of primary target sites on transgene silencing and transitivity using the GFP-expressing *Nicotiana benthamiana* 16C line, high pressure spraying protocol (HPSP), and synthetic 22-nucleotide (nt) long siRNAs. We found that the 22-nt siRNA targeting the 3' of the GFP transgene was less efficient in inducing silencing

when compared to the siRNAs targeting the 5' and middle region of the GFP. Moreover, sRNA sequencing of locally silenced leaves showed that the amount but not the profile of secondary RNAs is shaped by the occupancy of the primary siRNA triggers on the target RNA. Our findings suggest that RDR6-mediated dsRNA synthesis is not primed by primary siRNAs and that dsRNA synthesis appears to be generally initiated at the 3' end of the target RNA.

SIGNIFICANCE STATEMENT

This work answers a long-standing question about the role of siRNA triggers in initiating transitive silencing. By using high-pressure spraying-mediated delivery of synthetic siRNAs, we provided experimental evidence that target position of 22-nt-long primary siRNAs influences the efficiency of RDR6-driven double stranded RNA (dsRNA) synthesis, but it does not change the profile of accumulating secondary siRNAs originating from processing of RDR6-produced dsRNA.

INTRODUCTION

In plants, RNA interference (RNAi) plays a critical role in transcriptional regulation, genome stability and pathogen defense. RNAi machinery is initiated by double stranded RNAs (dsRNAs) in the cell. DsRNAs are processed by the endonucleases DICER-LIKE 4 (DCL4), DCL2 and DCL3 into 21-, 22- and 24-nt siRNAs, respectively (Deleris et al. 2006; Fusaro et al. 2006; Blevins et al. 2006). In general, 21-nt siRNAs are loaded onto AGO1 and cleave complementary transcripts, in a process termed post-transcriptional gene silencing (PTGS) (Hamilton and Baulcombe 1999). 22-nt siRNAs are also loaded onto AGO1 and are involved in either the onset of transitivity (Chen et al. 2010; Cuperus et al. 2010) or translational inhibition (Wu et al. 2020). Finally, 24-nt siRNAs are generally loaded onto AGO4 and the resulting complex is transported into the nucleus, where it reinforces RNA-directed DNA

54 methylation (RdDM) (Chan et al. 2004; Dalakouras and Wassenegger 2013; Wassenegger et
55 al. 1994).

56 An enzyme of paramount importance in plant RNAi is RNA-DIRECTED RNA
57 POLYMERASE 6 (RDR6). According to a mechanism termed sense-PTGS (S-PTGS), RDR6
58 is recruited onto aberrant RNAs (abRNAs) if the abRNA amount exceeds a certain threshold.
59 The resulting primary dsRNAs are processed into siRNAs, initiating target RNA silencing
60 (Parent et al. 2015; Wassenegger and Krczal, 2006). In addition, it has been demonstrated
61 that RDR6 is recruited to transcripts that are targeted by (primary) siRNAs for the generation
62 of dsRNA and secondary siRNAs, which map upstream and downstream of the primary
63 siRNA site, a process termed transitivity (Bleys et al. 2006a; Bleys et al. 2006b; Koscianska
64 et al. 2005; Montgomery et al. 2008a; Montgomery et al. 2008b; Vaistij and Jones 2009;
65 Vaistij et al. 2002; Vermeersch et al. 2010; Vermeersch et al. 2013; Moissiard et al. 2007;
66 Mlotshwa et al. 2008; Chen et al. 2010; Cuperus et al. 2010; Manavella et al. 2012, Sakurai et
67 al. 2021).

68 A growing body of evidence suggests that the onset of transitivity is influenced by the
69 nature of the target transcript. Indeed, transcripts originating from intron-containing genes are
70 poor substrates for RDR6 compared to those derived from intronless ones (Christie et al.
71 2011a; Christie and Carroll 2011; Christie et al. 2011b; Dadami et al. 2014; Dadami et al.
72 2013; Liu and Chen 2016; Vermeersch et al. 2010). In addition, transcript expression levels,
73 as well as regulatory elements at the promoter, and/or terminator sequence have been
74 implicated in the efficiency of transitivity (de Felippes and Waterhouse 2020). As noted
75 before, RDR6 transcribes abRNAs, which are devoid of 5′ cap and/or 3′ polyadenylation tail
76 (Gazzani et al. 2004; Luo and Chen 2007; Parent et al. 2015). AbRNAs may be produced by
77 both intronless and intron-containing genes e.g. upon read-through transcription or misplicing.
78 In the first case, the abRNAs are processed by RDR6, while in the second case, spliceosome
79 association seems to preferentially recruit the exonucleolytic RNA quality control for their

80 degradation (Christie et al. 2011a; Elvira-Matelot et al. 2016; Tsuzuki et al. 2017; Dalakouras
81 et al. 2019).

82 Along with the intrinsic features of the target transcript, the sRNA trigger itself appears
83 to affect the initiation and efficiency of transitive silencing. It has been suggested that sRNAs
84 with a size of 22-nt (Chen et al. 2010) or sRNAs containing an asymmetric bulge in their
85 duplex (Manavella et al. 2012) are changing AGO1 conformation thereby recruiting RDR6 to
86 their target, most likely with the aid of mediators such as SDE3 (Garcia et al. 2012), SDE5,
87 and SGS3 (Sakurai et al. 2021). In line with this, DCL2, responsible for the generation of 22-
88 nt siRNAs, is required for transitivity initiation (Mlotshwa et al. 2008). Yet, whether 22-nt
89 sRNAs mediate target cleavage, besides RDR6 recruitment, remains elusive. Previous reports
90 suggested that RNA cleavage is required for transitivity (Carbonell et al. 2012; Yoshikawa et
91 al. 2005). However, other studies challenge this assumption, arguing that cleavage is
92 dispensable for the onset of transitivity (Arribas-Hernandez et al. 2016; de Felippes et al.
93 2017).

94 RDR6 is postulated to initiate transcription predominantly from the very 3′ of the target
95 transcript (Schiebel et al. 1993) and not from an internal site, e.g. the siRNA cleavage site
96 (Moissiard et al. 2007). Furthermore, it has been shown that the 3' cleavage fragment of the
97 abRNA predominantly contributes to the RDR6-mediated transitivity. In contrast, the 5'
98 cleavage fragment, lacking a polyA tail, is subjected to exosome degradation after cleavage,
99 preventing its transcription by RDR6 (Branscheid et al., 2015; Yu et al., 2015). Transitivity
100 spreads both upstream and downstream of the primary siRNA site (Chen et al. 2010;
101 Manavella et al. 2012; McHale et al. 2013; Montgomery et al. 2008b). Yet, transitive
102 spreading is not indefinite, since RDR6 seems to reach its transcriptional limits after
103 approximately 700 nt (Axtell et al. 2006; Moissiard et al. 2007).

104 Despite considerable progress, the exact mode of action of sRNAs on transitivity
105 remains largely unaddressed (de Felippes and Waterhouse 2020). This is because transitivity

106 studies in plants have been based so far on (1) transgenes expressing hairpin RNAs (hpRNAs)
107 or inverted repeats (IRs), which are processed into a plethora of siRNAs, undermining any
108 attempt to allocate specific roles to discrete siRNAs (Bleys et al. 2006a; Bleys et al. 2006b;
109 Koscianska et al. 2005; Vaistij et al. 2002; Vermeersch et al. 2010; Vermeersch et al. 2013),
110 (2) endogenous micro RNAs (miRNAs), which induce transitivity at very specific
111 endogenous loci and thus exhibit a mode of action hardly reflecting a more generalized
112 process (Axtell et al. 2006; Montgomery et al. 2008a; Montgomery et al. 2008b), and (3)
113 artificial miRNAs (amiRNAs), whose artificial long RNA precursor molecules are generally
114 misprocessed into more than a single amiRNA (Chen et al. 2010; Cuperus et al. 2010;
115 Manavella et al. 2012; McHale et al. 2013). In order to tackle incongruence and investigate
116 the onset and establishment of transitivity triggered by discrete/unique sRNAs, in this study *in*
117 *vitro* synthesized 22-nt siRNAs targeting the 5', middle and 3' of a GREEN FLUORESCENT
118 PROTEIN (GFP) transcript were exogenously delivered by High Pressure Spraying Protocol
119 (HPSP) in the GFP-expressing *Nicotiana benthamiana* 16C plant line (Dalakouras et al. 2016;
120 Uslu et al. 2020). The data presented in this study provide novel insights of the mechanistic
121 details of transitivity in plants.
122
123 **RESULTS**
124 **SiRNAs targeting 5'-GFP and mid-GFP regions display stronger silencing than 3'-GFP.**
125 We monitored silencing efficiency using the GFP transgene in the *Nicotiana benthamiana*
126 16C line (Nb-16C) (Voinnet and Baulcombe 1997). We designed three 22-nt long siRNAs
127 (siRNA#164, siRNA#386, and siRNA#739) targeting the 5', middle, and 3' regions of the
128 GFP, respectively (Figure 1a). Each siRNA consists of a double stranded RNA with a 20-nt
129 overlapping sequence, a 5'-phosphate and 2-nt overhangs at the 3' sides, which were not
130 methylated. The overlapping sequences possess a uracil-adenine pairing at the end to ensure
131 an effective AGO1 loading (Czech et al. 2009) (Figure 1a). We applied siRNAs on Nb-16C

132 leaves via HPSP and local silencing phenotypes were evaluated 6 days post spraying (6 dps).
133 17 out of 17 of the siRNA#164- and siRNA#386-sprayed Nb-16C plants (16C-siR164 and
134 16C-siR386) showed strong and consistent local silencing. In contrast, 14 out of 17 of the
135 siRNA739-treated plants (16C-siR739) had relatively mild silencing phenotypes, and 3 out of
136 the 17 16C-siR739 displayed no GFP silencing, at all (Figure 1b). When the strength of local
137 silencing is evaluated by the ratio of silenced areas to the whole leaf area, we found that 16C-
138 siR164, 16C-siR386, and 16C-siR739 lead to 45%, 35%, and 7% silenced areas in average,
139 respectively (Figure S1). Systemic silencing phenotypes were evaluated at 35 dps; 15 out of
140 17 16C-siR164, 13 out of 17 16C-siR386, and only 1 out of 17 of the 16C-siR739 plants
141 showed systemic silencing (Figure 1c). Hence, 22-nt siRNAs targeting the 5'-GFP and mid-
142 GFP regions resulted in significantly more efficient local ($p<10^{-3}$ with Student's t-test based
143 on silenced areas) and systemic ($p<10^{-4}$ with Fishers exact test based on the number of
144 systemically silenced plants) transgene silencing than the 22-nt siRNAs targeting the 3' GFP
145 region.
146
147 **The level of silencing efficiency of siRNAs is independent of the target site accessibility**
148 In order to exclude that the recorded difference in silencing efficiency between the 5'- and 3'-
149 mapping 22-nt siRNAs was not due to differential AGO loading and/or GFP target
150 accessibility by these siRNAs we used 21-nt siRNAs exactly matching to siRNA#164 and
151 siRNA#739 sequence with one missing nucleotide at the 3'end of the top strand and 5'end of
152 the bottom strand (named as siRNA#164-21, siRNA#739-21, respectively) (Figure 2a). These
153 21-nt siRNAs were delivered via HPSP and 6 days post spraying 5 out of 6 Nb-16C displayed
154 local silencing phenotype for both siRNA#164-21 and siRNA#739-21 (Figure 2b). The level
155 of silencing based on the silent areas and the number of plants displaying a silencing
156 phenotype were indistinguishable between siRNA#164-21nt and siRNA#739-21nt (Figure 2c).
157 In addition, we agroinfiltrated Nb-16C with 21-nt GFP amiRNA constructs targeting regions

158 in the close proximity of siRNA#164 and siRNA#739 and observed that both 5' and 3'
159 amiRNAs lead to a similar level of silencing at 8 days post infiltration (Figure S2).
160 Collectively, the 21-nt siRNA spraying and 21-nt amiRNA agroinfiltration assays strongly
161 suggested that the GFP target is equally susceptible at its 5' and 3' regions to small RNAs.
162 Thus, the reasons for the discrepancy of silencing efficiency upon spraying of 5' and 3'-
163 mapping 22-nt siRNAs seem to lie elsewhere.
164

165 **22-nt siRNA occupancy influences the amount of secondary siRNAs but not the**
166 **transitivity hotspots**

167 It is well known that silencing efficiency is positively correlated to transitivity levels. We thus
168 reasoned that the discrepancy in silencing efficiency among the 5', middle and 3' 22-nt
169 siRNAs could reflect differences in the corresponding levels of transitivity onset. In order to
170 investigate this, we performed sRNA sequencing (sRNA-seq) using leaf samples showing
171 local silencing at 6 dps. SRNA-seq revealed the presence of 21-, 22-, and 24-nt secondary
172 sRNAs mapping to the GFP sequence on both strands outside of the regions targeted by
173 sprayed 22-nt siRNAs demonstrating that all three 22-nt siRNAs led to transitive silencing as
174 early as 6 dps (Figure 3a). The combined normalized profiles of 21-, 22-, and 24-nt long
175 sRNAs in a sliding window of 10-nt revealed multiple secondary siRNA hotspots shared
176 among the different siRNA treatments (see Materials and Methods, sRNA-seq normalization)
177 (Figure 3a). The qualitative profile of sRNA reads obtained by percentage density distribution
178 (pdd, see Materials and Methods, sRNA-seq quantification) also showed several perfectly
179 matching hotspots (Figure 3b). The most prominent secondary siRNA hotspot (Transitivity
180 Hot Spot, THS) appeared as two adjacent peaks between positions +541 and +577 of the GFP
181 cDNA, fully overlapping for all three siRNA treatments (Figure 3a, 3b). Despite the matching
182 hotspots, siRNA#164 treatment compared to siRNA#386 and siRNA#739, and siRNA#386
183 treatment compared to siRNA#739 produced significantly higher amounts of transitive

184 siRNAs, when compared to siRNA#386 and siRNA#739 ($p<10^{-5}$) (Figure 3c). The average
185 distance between two transitivity peaks was measured 23.8bp (Figure 3d).
186
187 **Primary 22-nt siRNA target sites do not influence secondary siRNA distribution**
188 In order to find out whether primary 22-nt siRNA binding sites shape the secondary sRNA
189 distribution, we divided the GFP cDNA into 6 regions: 5' region of the siRNA#164 (1-164),
190 the regions between siRNA#164 and siRNA#386 (165-386), siRNA#386 and THS region
191 (387-540), THS and siRNA#739 region (578-739), 3' region of siRNA#739 (740-772), and
192 the THS region (541-577) itself. The regional percentage distribution of the sRNA-reads (rpd-
193 sRNA, see Materials and Methods, sRNA-seq quantification) showed that in the region 1-164,
194 which was 612 bp upstream from the 3'end of the GFP cDNA, contains less than 1% of the
195 reads for all siRNA treatments and there was no statistical difference when different
196 treatments were compared (Figure 4a). A significantly higher portion of secondary siRNAs in
197 16C-siR164 mapped to the region 165-386 when compared to those of 16C-siR386 and 16C-
198 siR739 ($p<10^{-3}$). In the 387-540 region, siRNA#164 treatment lead to significantly higher
199 percentage of reads when compared to siRNA#739 but not to siRNA#386 ($p<0.05$).
200 Interestingly, the percentage distribution of the reads in the THS did not differ among the
201 siRNA treatments. On the other 3' side of the THS, 16C-siR164 had significantly lower ratio
202 of reads in the 578-739 region, than 16C-siR386 and 16C-siR739 ($p<10^{-3}$) (Figure 4a). Since
203 these regions are different in length, we calculated the average read density per base pair
204 (ARDBP) for each treatment (see Materials and Methods, sRNA quantification) (Figure 4b).
205 None of the siRNA treatments lead to a specific enrichment or depletion on the 5' side of their
206 primary target site when compared to the 3' side (Figure 4b). For all three siRNAs treatments,
207 the transitive siRNA distribution per base pair was the highest in THS and ARDBP decreased
208 both on 5' and 3' sides of the THS as the distance of the region to THS increased (Figure 4b).
209 It needs to be noted here that even simple water spraying on Nb-16C yielded solely sense

210 strand sRNAs due to GFP degradation (Uslu et al. 2020). Namely, the sense strand sRNAs we
211 obtained upon 22-nt siRNA spraying was a combination of both secondary siRNAs and GFP
212 degradation products, whereas the antisense sRNAs must be solely considered as RDR6
213 transcription products. Therefore, strand specific ARDBP (ssARDBP) was used to distinguish
214 the contribution of sense and anti-sense strands. SsARDBP showed that in regions 164-386,
215 387-540 and 578-739 of 16C-siR164 and 16C-siR386, mainly antisense secondary siRNAs
216 contributed to minor but statistically significant differences in secondary siRNA enrichment
217 when compared to 16C-siR739 (Figure 4c). Hence, despite having mild differences in the
218 secondary siRNA enrichment between the 5' and 3' side of the THS upon different treatments,
219 the overall distribution of secondary siRNAs remained identical in all treatments (Figure 4b,
220 Figure S3).
221
222 **The size distribution of secondary siRNAs was not affected by the primary siRNA target**
223 **site**
224 The raw read counts of 21-, 22- and 24-nt reads mapping to the GFP were compared to 21-nt
225 reads mapping to the GFP. 22-nt reads were approximately one third and 24-nt reads were
226 approximately one seventh of the 21-nt reads in all siRNA treatments regardless of the strand
227 polarity (Figure 5a). In corroboration with previous findings, the cleavage process appeared to
228 have a preference for DCL4, DCL2, and DCL3, in this order (Kumakura et al. 2009; Pontes et
229 al. 2013). However, the ratio of 21-nt transitive siRNA reads (normalized to all 21-nt long
230 reads) were equal to the 22-nt secondary siRNAs reads (normalized to all 22-nt reads) in all
231 treatments (Figure 5b), suggesting that DCL preference (DCL4>DCL2>DCL3) did not
232 change from early to late stages of transitivity. In siR164, 21- and 22-nt reads contributed to
233 THS equally. However, the 22- to 21-nt ratio in THS in siR164 decreased in siR386 samples
234 and decreased even further in siR739 samples (black arrows, Figure 6a, 6b). There are
235 multiple peaks like THS, which were more prominent on the sense strand in all treatments

236 (black arrows, Figure 6a). Besides, there were a few peaks on the sense strand, specific to 22-
237 nt reads, which were completely absent in the anti-sense strand (purple arrow, Figure 6b).
238 Although the most abundant secondary siRNA read in THS had a 5' uracil for majority of the
239 samples, taking top 5 or top 10 highly represented reads into consideration, we did not detect
240 any particular sequence feature or motif, which might underlie differential representation of
241 the reads on the sense and the anti-sense strands.
242
243 **DISCUSSION**
244 Transitive silencing has been well studied before, but its induction was never analyzed by
245 using unique/discrete siRNAs. We have previously shown that upon HPSP, 22-nt siRNAs
246 were the most potent inducers of local and systemic silencing when compared to 21-nt and
247 24-nt siRNAs (Dalakouras et al. 2016). In this study, we used 22-nt siRNAs targeting
248 different regions of the GFP transgene in the Nb-16C line to analyze the onset of transitivity
249 by sRNA-seq. Overall, our data showed that 22-nt siRNAs targeting the 5', middle and 3' of
250 the GFP, all induced local silencing at different levels (Figure S1).
251 The efficiency of transitivity (in terms of the quantity of secondary siRNAs produced)
252 was positively correlated with the gradual proximity of the siRNA trigger towards the 5' of
253 the target (see below). It has been demonstrated before that the generation of secondary
254 dsRNAs/siRNAs not only amplifies/reinforces local silencing, but also mediates the
255 surpassing of a certain threshold required for the onset of systemic silencing (Kalantidis et al.
256 2006). Indeed, we observed that the gradual siRNA proximity to the 5' led to not only more
257 efficient transitivity but also to more efficient establishment of systemic silencing. These data
258 suggest that transitivity and systemic silencing are tightly connected, although the RNA
259 molecule serving as the actual mobile signal still needs to be identified.
260 Having a closer look at the generation of the secondary siRNA profiles in the locally
261 silenced tissue provides some interesting insights regarding the mechanistic details of

262 transitivity. (1) All sprayed 22-nt siRNAs triggered transitivity towards both their 5' and 3',
263 demonstrating that siRNA-mediated transitivity is bi-directional and not uni-directional
264 (Vaistij et al. 2002). (2) Despite targeting different regions on the GFP transcript,, the three
265 applied 22-nt siRNAs produced very similar transitivity patterns, suggesting that they were
266 not used as primers for RDR6 (otherwise transitivity would have spread only towards the 5'
267 upstream region of each siRNA trigger), corroborating previous reports (Moissiard et al.
268 2007). (3) In all three 22-nt siRNA applications, RDR6 transcription started from the very 3'
269 region of the transcript and proceeded towards the 5' for approximately 700 nt (since very few
270 secondary siRNAs were detected in the 1-168 region), again in line with previous reports
271 (Moissiard et al. 2007). (4) The homogeneity of the transitivity pattern in all three cases
272 suggests that the starting point from which RDR6 initiated transcription referred to the very 3'
273 region of non-cleaved target transcripts, and not to the 3' end fragments that are generated by
274 RISC-mediated cleavage. Moreover, prematurely terminated transcripts of the GFP that could
275 be considered as abRNA are unlikely serving as templates for RDR6. Accordingly, the role of
276 22-nt siRNAs would be to predominantly recruit RDR6 to the 3' end of the target rather than
277 mediate target RNA cleavage (Figure 7). Indeed, 22-nt siRNAs and/or siRNAs exhibiting an
278 asymmetric bulge at their duplex were supposed to change AGO1 conformation (Manavella et
279 al. 2012). This new conformation could not only impair AGO1's RNase activity but could
280 also recruit RDR6 to the 3' of the target transcript, conceivably with the aid of mediators such
281 as SDE3 and SGS3 (Garcia et al. 2012, Sakurai et al. 2021). Although 22-nt miRNAs are
282 demonstrated to cleave the target RNAs, our study shows 22-nt siRNAs have evidently a
283 different mode of action than 22-nt miRNAs. We are unaware why this might be so, but it
284 should be taken into consideration that siRNAs and miRNAs share neither the same
285 biogenesis pathway (e.g. different DCLs and other protein partners involved) nor identical
286 biochemical properties (e.g. miRNAs may contain asymmetric bulges whereas siRNAs are
287 perfect duplexes) (5) The accumulating secondary siRNAs were predominantly of 21-nt in

288 size, followed by 22-nt siRNAs and only negligible numbers of 24-nt siRNAs. These findings
289 were in line with previous reports showing that, while all DCLs predominantly co-localize in
290 the nucleus, DCL4 is also present in the cytoplasmic SGS3/RDR6 bodies, thus having
291 privileged access to the RDR6-produced dsRNA (Kumakura et al. 2009; Pontes et al. 2013).
292 (6) Investigating the polarity of secondary siRNA reads, we recorded that they were mainly of
293 sense rather than antisense polarity (compared to the sense target). The reasons for this
294 observation are not very clear, but we speculate that antisense strands, loaded onto AGO1 and
295 exhibiting cleavage activity on the sense target are degraded post-cleavage, while sense
296 strands, having no obvious target in the cell, have a longer half-life (Shi et al., 2020). (7) The
297 fact that no U-only or A-only sRNA reads were detected (which could have been derived
298 from DCL processing of an A/U-only dsRNA) suggests that RDR6 does not process polyA-
299 containing mRNAs. It has been demonstrated that polyA inhibits RDR6 (Baeg et al. 2017).
300 Moreover, it was shown that RDR6 prefers non-polyadenylated transcripts (Luo and Chen
301 2007). Indeed, RDR6 transcription of polyA would generate U-only siRNAs that could
302 indiscriminately target any polyA-containing mRNA for cleavage, with devastating effects for
303 the plant cell (Dalakouras et al. 2019). Thus, we suggest that in our case, the sprayed 22-nt
304 siRNAs targeted both GFP mRNAs and GFP abRNAs, but seemingly did not efficiently
305 cleave them. To the GFP mRNA, the 22-nt siRNA failed to recruit RDR6 due to the presence
306 of the polyA, but inhibited its translation (Wu et al. 2020). To the GFP abRNA, RDR6 could
307 be recruited to initiate S-PTGS. However, the Nb-16C line does not show spontaneous
308 silencing indicating that the concentration of abRNA is too low for the initiation of S-PTGS.
309 The presence of 22-nt siRNAs appears to kinetically facilitate RDR6 recruitment to abRNA,
310 culminating in the generation of secondary 21-nt siRNAs that targeted both GFP mRNA and
311 GFP abRNA for degradation and reinforcement of silencing state (Figure 7). Besides, the 22-
312 nt siRNA mapping to the 3' end of the GFP transcript well may pose a steric hindrance for
313 RDR6 recruitment, which underlies weak local and systemic silencing (Figure 7).

314 Introducing pure siRNAs to plants via HPSP allows exploring the mechanistical
315 aspects of RNAi and transitivity in an unprecedented clarity. Nevertheless, further studies
316 employing spraying of siRNAs of variable biochemical properties in RNAi-deficient mutants
317 would shed additional light in the elusive nature of transitive and systemic silencing.
318
319
320 **EXPERIMENTAL PROCEDURES**
321 **High Pressure Spraying Protocol (HPSP)**
322 14 of 25 days old *Nicotiana benthamiana* 16C (Nb-16C) plants were used for spraying. Given
323 siRNAs (Figure 1a, 2a) are synthesized by Metabion (www.metabion.com) and dissolved in
324 water. For each plant 200µl of aqueous siRNA solution at 1µM concentration is sprayed from
325 a 0.5-1 cm distance at the shoot apical meristem and at the abaxial surface of the leaves with
326 an airbrush pistol (CONRAD AFC-250A, 0.25mm nozzle). 5-6 bar pressure is provided by
327 the METABO Elektra Beckum Classic 250 compressor for spraying (www.metabo.com). For
328 each siRNA a separate unused airbrush is used to prevent cross-contamination. Furthermore,
329 at the times of spraying only one set of plants (14 Nb-16C and 3 Nb-16C) were present in the
330 room and they were covered with a transparent plastic hood subsequent to spraying to prevent
331 siRNA cross-contamination through aerosols.
332
333 **Ultraviolet (UV) Monitoring**
334 GFP expressing Nb-16C plants were visualized 6 days post spraying (dps) and 35 dps under
335 UV light (Blak-Ray B-100 AP Lamp, www.uvp.com). Images were taken using a Canon
336 EOS700D (18-55mm), aperture priority mode (A=10). First systemic silencing appeared 14
337 dps and GFP monitoring was weekly performed up to 60 dps.
338
339 **RNA Extraction and Small RNA Sequencing**

340 6 dps, 1 leaf per plant from three plants were pooled as one biological replicate of an sRNA-
341 seq sample. The silenced parts of the leaves were cut out. Three samples per siRNA spraying
342 were collected. The other sprayed leaves were left on the plant to monitor the development of
343 systemic silencing. SRNAs were extracted by mirVana miRNA extraction kit according to
344 manufacturer's instructions (www.thermofisher.com). 250 ng of RNA per biological replicate
345 were provided to GenXPro GmbH for sRNA-seq. GenXPro used TrueQuant SmallRNA Seq
346 Kit for library preparation (https://genxpro.net/). Illumina NextSeq500 instrument was used
347 for sequencing the libraries with 75 cycles of sequencing. As expected from previous reports,
348 sRNA-seq quality control show that 24- and 21-nt reads are the most abundant reads (Table
349 S1, Blevins et al. 2015, Uslu et al. 2020).
350
351 **Bioinformatic Analysis**
352 SRNA-seq reads are mapped to the GFP sequence of the Nb-16C (Philips et al., 2017). The
353 bam files are visualized on TABLET® (Milne et al. 2013) and the following data processing
354 and line charts/bar graphs have been plotted using Microsoft Excel.
355
356 **Elimination of aerosol based cross-contamination upon spraying**
357 When siRNAs are sprayed not all of them enter the plant cells and most likely, the majority of
358 them stick to the surface of the leaves. In addition, a reasonable number of siRNAs will, as
359 aerosolic particles, contaminate other non-sprayed plants. Despite all efforts to block cross-
360 contamination via aerosols upon spraying, in all plants we could still detect siRNAs, which
361 were not sprayed to this particular plant but some others. In order to assess the contribution of
362 this aerosol based cross contamination, we sprayed 3 Nb-16C plants with an siRNA mapping
363 to the promoter sequence of the GFP (siRNA-35S). Upon sequencing of these control plants,
364 we could detect previously sprayed siRNAs, namely siRNA#164, siRNA#386, siRNA#739.
365 However, we never monitored any contamination-related GFP silencing, in corroboration

366 with our previous data (Uslu et al. 2020). Moreover, sRNA-seq data of siRNA-35S-sprayed
367 (data not shown) and water-sprayed (Uslu et al. 2020) Nb-16C samples did not reveal
368 secondary siRNAs or any other anti-sense sRNA mapping to the GFP sequences. This
369 suggests that the contaminating siRNAs did not contribute to transitivity. In order to focus on
370 the secondary siRNAs only, we eliminated all reads mapping to siRNA164, siRNA386, and
371 siRNA739. It should be noted that the sprayed siRNAs represented the far most (91% to 98%)
372 of all reads mapping to the GFP. This underpins the assumption that most of the sprayed
373 siRNAs stick to the leaf surface.
374
375 **SRNA-seq Normalization**
376 Since there are currently no established protocols for normalizing the reads, we used
377 miRNA159 abundance, average and geometric average reads of 3 independent miRNAs,
378 sprayed siRNA abundance, total number of reads, total number of 21-nt reads, total GFP
379 sense reads, NOS terminator reads as a reference to normalize the sRNA reads mapping to the
380 GFP. However, the variance among biological replicates was too high to obtain any
381 meaningful comparison between different treatments. Finally, we normalized sRNAs mapping
382 to the GFP sequence with the total number of sRNAs of given size. Namely, 21-nt long reads
383 mapping to the GFP were normalized to the number of all 21-nt reads (Table S1). We
384 obtained the lowest variance among biological replicates using this size-based normalization.
385 Normalized average read counts refer to this number multiplied with 10^6 (Figure 2a, 2c, 4b, 5).
386
387 **SRNA-seq quantification**
388 Percent density distribution (pdd) is calculated by dividing the sum of 21-, 22-, and 24-nt
389 reads mapping to the given position to the total number of 21-, 22-, and 24-nt reads mapping
390 to the GFP (Figure 2b). Pdd gives an accurate comparison of the distribution of secondary
391 siRNAs among different treatments, allowing us to compare the treatments qualitatively,

392 regardless of the total abundance of transitive siRNAs. Regional percent distribution of 21-,
393 22-, 24-nt reads (rpd-sRNA) is obtained by dividing the number of 21-, 22-, and 24-nt reads
394 mapping to the region of interest given in the X-axis to the total number of 21-, 22- and 24-nt
395 reads mapping to the GFP. However, we obtain higher values of rpd-sRNA for larger regions.
396 In order to avoid the size-bias, we calculated average read density per base pair (ARDBP).
397 For ARDBP, we normalized strand specific rpd-sRNA for each region given in the X-axis by
398 the size of the region. ARDBP allows comparison of transitivity distribution of different
399 treatments in a quantitative manner (Figure 4b). The abundance of 21-, 22-, and 24-nt long
400 sRNAs are compared by simply dividing the raw read counts of the sRNAs mapping to GFP
401 to the raw read counts of the 21-nt long sRNAs mapping to GFP (Figure 5a). Next, we
402 evaluated the abundance of 21-, 22-, and 24-nt sRNAs mapping to the GFP normalized with
403 the total number of corresponding size sRNA along the GFP (Figure 5b)
404
405 **Statistical Tests**
406 The statistical comparison of systemic silencing efficiency among different treatments were
407 performed by Fisher's Exact Test with a significance threshold of $p<0.001$ (Figure 1c). The
408 statistical analysis pdsRNA, ARDBP, and pdd are performed by pairwise comparisons using
409 Student's t-test. The significance thresholds are: $p<0.05$(*), $p<0.01$(**), and $p<0.001$(***).
410
411 **Quantification of Silencing Efficiency.**
412 Western Blot and RNA quantification-based biochemical methods are not sensitive enough to
413 detect silencing for the following three reasons. (1) HPSP causes wounding of the cells, which
414 in turn change the transcript and protein level GFP and the genes for normalization. (2) The
415 sample collection area is heterogeneous, and it is not possible to isolate the silenced areas
416 very precisely. (3) At 6dps the silencing efficiency is too low (1-10%) to quantify reliably by
417 biochemical methods. Therefore, local silencing efficiency is evaluated by comparing the area

418 of silenced section to the rest of the leaf. For RGB images, the silenced area and the whole
419 leaf area are manually marked by "Freehand Selections" tool on FIJI (www.imagej.net). The
420 area is measured by "Measure" tool on FIJI. The silenced area value is divided by the whole
421 leaf area. The resulting value is multiplied by hundred for the percent silencing efficiency. For
422 32-bit images, an auto threshold is applied on the GFP channel and far red channel, while the
423 zero values are assigned as NaN. The GFP area is divided by far red channel area to find non-
424 silenced area (NSA). The percent silencing efficiency is quantified as (1-NSA)*100.
425
426 **Generation of artificial miRNA constructs.**
427 The artificial miRNA constructs designed to target GFP and to contain the Ath-miR319a
428 backbone were synthesized by Life Technologies and delivered cloned into pMA-T vector
429 (www. thermofisher.com). Then, the amiRNA cassette was *Xho*I/*Nco*I cloned into pG104
430 binary vector and introduced into ATHV agrobacteria for agroinfiltration, as described before
431 (Dadami et al. 2013).
432
433 **ACCESSION NUMBERS**
434 The data discussed in this publication have been deposited in NCBI's Gene Expression
435 Omnibus (Edgar et al., 2002) and will be accessible through GEO Series accession number
436 upon reviews' request.
437
438 **Author Contributions**
439 VVU, GK, AD and MW conceived the experiments and wrote the manuscript. VVU and
440 conducted the experiments and analyzed the data, unless otherwise is indicated. AD
441 performed the cloning and the agroinfiltration of amiRNA constructs. VAS contributed to the
442 bioinformatic analysis of the sRNA-seq. All authors contributed to the article and approved
443 the submitted version.

444

445 **Funding**

446 Funding of this project was provided by the German Research Foundation (DFG), Grant:
447 Wa1019/14-1 and by the Federal Ministry of Education and Research (BMBF), Grant:
448 03180531.

449

450 **Conflict of Interest**

451 The authors declare that the research was conducted in the absence of any commercial or
452 financial relationships that could be construed as a potential conflict of interest.

453

454 **SHORT LEGENDS FOR SUPPORTING INFORMATION**

455 **Supplementary Table 1| sRNA-seq quality control**. Total read numbers and 21, 22, and
456 24nt read numbers given in the table. In addition, the 22nt reads matching exactly to sprayed
457 RNAs are provided.

458

459 **Supplementary Figure 1| The comparison of silenced among 22-nt siRNA treatments**.
460 The images of 9 leaves per treatment, which were used for sRNA-seq, were captured as RGB
461 image. The silenced red areas were quantified and compared to the whole leaf area. siR164
462 and siR386 have significantly larger silenced areas than siR739 ($p<0.001$).

463

464 **Supplementary Figure 2| AmiRGFP constructs design and function upon**
465 **agroinfiltration in Nb-16C**. Schematic representation of constructs: P^{35S}: CaMV 35S
466 promoter, T^{35S}: CaMV 35S terminator; T^{NOS}: nopaline synthase (NOS) terminator; GFP:
467 green fluorescence protein; amiRGFP5´: artificial miRNA targeting the 5´ region of GFP
468 (138-158 bp); amiRGFP3´: artificial miRNA targeting the 3´ region of GFP (672-692 bp).
469 Transcription of the aMIRGFP transgene generates pri-amiRGFP (not depicted) that is

470 processed to pre-amiRGFP. Ideally, DCL1 processing of the latter produces the 21-bp
471 amiRGFP:amiRGFP* duplex that has 2-nt 3′ overhangs. However, processing by additional
472 DCLs cannot be excluded (not depicted). Mismatches that generates symmetric bulges in the
473 pre-amiRGFP and amiRGFP:amiRGFP* molecules are indicated with open boxes. In red, the
474 sequence of the single stranded 21-nt amiRGFP. Upon agroinfiltration, amiRGFP 5' and
475 amiRGFP 3' target the GFP transcript at positions 138-158 bp and 672-692 bp, respectively,
476 and cleave it (loss of GFP expression upon ultraviolet examination 8 days post
477 agroinfilration).
478
479 **Supplementary Figure 3| Comparison of abundance of secondary siRNAs according to**
480 **their position with respect to THS.** The normalized 21,22, and 24nt mapping to the 5' side
481 of the THS is normalized to the 3' side of the THS on both strands for three siRNA treatments.
482 (**, p<0.01)
483
484
485 **REFERENCES**

486 Arribas-Hernandez L, Marchais A, Poulsen C, Haase B, Hauptmann J, Benes V, Meister G,
487 Brodersen P (2016) The Slicer Activity of ARGONAUTE1 Is Required Specifically
488 for the Phasing, Not Production, of Trans-Acting Short Interfering RNAs in
489 Arabidopsis. The Plant cell 28 (7):1563-1580
490 Axtell MJ, Jan C, Rajagopalan R, Bartel DP (2006) A two-hit trigger for siRNA biogenesis in
491 plants. Cell 127 (3):565-577
492 Baeg K, Iwakawa HO, Tomari Y (2017) The poly(A) tail blocks RDR6 from converting self
493 mRNAs into substrates for gene silencing. Nat Plants 3:17036.
494 doi:10.1038/nplants.2017.36
495 Blevins T, Rajeswaran R, Shivaprasad PV, Beknazariants D, Si-Ammour A, Park HS,
496 Vazquez F, Robertson D, Meins F, Jr., Hohn T, Pooggin MM (2006) Four plant Dicers
497 mediate viral small RNA biogenesis and DNA virus induced silencing. Nucleic acids
498 research 34 (21):6233-6246
499 Blevins T, Podicheti R, Mishra V, Marasco M, Wang J, Rusch D, Tang H, Pikaard CS (2015)
500 Identification of Pol IV and RDR2-dependent precursors of 24 nt siRNAs guiding de
501 novo DNA methylation in Arabidopsis. Elife. 4:e09591.
502 Bleys A, Van Houdt H, Depicker A (2006a) Down-regulation of endogenes mediated by a
503 transitive silencing signal. RNA (New York, NY 12 (9):1633-1639

504 Bleys A, Vermeersch L, Van Houdt H, Depicker A (2006b) The frequency and efficiency of
505 endogene suppression by transitive silencing signals is influenced by the length of
506 sequence homology. Plant physiology 142 (2):788-796
507 Branscheid A, Marchais A, Schott G, Lange H, Gagliardi D, Andersen SU, Voinnet O,
508 Brodersen P (2015) SKI2 mediates degradation of RISC 5'-cleavage fragments and
509 prevents secondary siRNA production from miRNA targets in Arabidopsis. Nucleic
510 Acids Res. 43(22):10975-88. doi: 10.1093/nar/gkv1014.
511 Carbonell A, Fahlgren N, Garcia-Ruiz H, Gilbert KB, Montgomery TA, Nguyen T, Cuperus
512 JT, Carrington JC (2012) Functional analysis of three Arabidopsis ARGONAUTES
513 using slicer-defective mutants. The Plant cell 24 (9):3613-3629
514 Chan SW, Zilberman D, Xie Z, Johansen LK, Carrington JC, Jacobsen SE (2004) RNA
515 silencing genes control de novo DNA methylation. Science 303 (5662):1336.
516 doi:10.1126/science.1095989
517 Chen HM, Chen LT, Patel K, Li YH, Baulcombe DC, Wu SH (2010) 22-Nucleotide RNAs
518 trigger secondary siRNA biogenesis in plants. Proc Natl Acad Sci U S A 107
519 (34):15269-15274. doi:10.1073/pnas.1001738107
520 Christie M, Brosnan CA, Rothnagel JA, Carroll BJ (2011a) RNA decay and RNA silencing in
521 plants: competition or collaboration? Front Plant Sci 2:99
522 Christie M, Carroll BJ (2011) SERRATE is required for intron suppression of RNA silencing
523 in Arabidopsis. Plant Signal Behav 6 (12):2035-2037
524 Christie M, Croft LJ, Carroll BJ (2011b) Intron splicing suppresses RNA silencing in
525 Arabidopsis. Plant J 68 (1):159-167. doi:10.1111/j.1365-313X.2011.04676.x
526 Cuperus JT, Carbonell A, Fahlgren N, Garcia-Ruiz H, Burke RT, Takeda A, Sullivan CM,
527 Gilbert SD, Montgomery TA, Carrington JC (2010) Unique functionality of 22-nt
528 miRNAs in triggering RDR6-dependent siRNA biogenesis from target transcripts in
529 Arabidopsis. Nat Struct Mol Biol 17 (8):997-1003. doi:10.1038/nsmb.1866
530 Czech B, Zhou R, Erlich Y, Brennecke J, Binari R, Villalta C, Gordon A, Perrimon N,
531 Hannon GJ (2009) Hierarchical rules for Argonaute loading in Drosophila. Mol Cell.
532 13;36(3):445-56. doi: 10.1016/j.molcel.2009.09.028.
533 Dadami E, Dalakouras A, Zwiebel M, Krczal G, Wassenegger M (2014) An endogene-
534 resembling transgene is resistant to DNA methylation and systemic silencing. RNA
535 Biol 11 (7):934-941. doi:10.4161/rna.29623
536 Dadami E, Moser M, Zwiebel M, Krczal G, Wassenegger M, Dalakouras A (2013) An
537 endogene-resembling transgene delays the onset of silencing and limits siRNA
538 accumulation. FEBS letters 18 (587(6)):706-710
539 Dalakouras A, Lauter A, Bassler A, Krczal G, Wassenegger M (2019) Transient expression of
540 intron-containing transgenes generates non-spliced aberrant pre-mRNAs that are
541 processed into siRNAs. Planta 249 (2):457-468. doi:10.1007/s00425-018-3015-6
542 Dalakouras A, Wassenegger M (2013) Revisiting RNA-directed DNA methylation. RNA Biol
543 10 (3):453-455. doi:10.4161/rna.23542
544 Dalakouras A, Wassenegger M, McMillan JN, Cardoza V, Maegele I, Dadami E, Runne M,
545 Krczal G, Wassenegger M (2016) Induction of Silencing in Plants by High-Pressure
546 Spraying of In vitro-Synthesized Small RNAs. Front Plant Sci 7:1327.
547 doi:10.3389/fpls.2016.01327
548 de Felippes FF, Marchais A, Sarazin A, Oberlin S, Voinnet O (2017) A single miR390
549 targeting event is sufficient for triggering TAS3-tasiRNA biogenesis in Arabidopsis.
550 Nucleic acids research
551 de Felippes FF, Waterhouse PM (2020) The Whys and Wherefores of Transitivity in Plants.
552 Front Plant Sci 11:579376. doi:10.3389/fpls.2020.579376

553 Deleris A, Gallego-Bartolome J, Bao J, Kasschau KD, Carrington JC, Voinnet O (2006)
554 Hierarchical action and inhibition of plant Dicer-like proteins in antiviral defense.
555 Science (New York, NY 313 (5783):68-71
556 Elvira-Matelot E, Bardou F, Ariel F, Jauvion V, Bouteiller N, Le Masson I, Cao J, Crespi MD,
557 Vaucheret H (2016) The Nuclear Ribonucleoprotein SmD1 Interplays with Splicing,
558 RNA Quality Control, and Posttranscriptional Gene Silencing in Arabidopsis. The
559 Plant cell 28 (2):426-438
560 Fusaro AF, Matthew L, Smith NA, Curtin SJ, Dedic-Hagan J, Ellacott GA, Watson JM, Wang
561 MB, Brosnan C, Carroll BJ, Waterhouse PM (2006) RNA interference-inducing
562 hairpin RNAs in plants act through the viral defence pathway. EMBO Rep 7
563 (11):1168-1175. doi:10.1038/sj.embor.7400837
564 Garcia D, Garcia S, Pontier D, Marchais A, Renou JP, Lagrange T, Voinnet O (2012) Ago
565 hook and RNA helicase motifs underpin dual roles for SDE3 in antiviral defense and
566 silencing of nonconserved intergenic regions. Mol Cell 48 (1):109-120.
567 doi:10.1016/j.molcel.2012.07.028
568 Gazzani S, Lawrenson T, Woodward C, Headon D, Sablowski R (2004) A link between
569 mRNA turnover and RNA interference in Arabidopsis. Science 306 (5698):1046-1048.
570 doi:10.1126/science.1101092
571 Hamilton AJ, Baulcombe DC (1999) A species of small antisense RNA in posttranscriptional
572 gene silencing in plants. Science 286 (5441):950-952
573 Kalantidis K, Tsagris M, Tabler M (2006) Spontaneous short-range silencing of a GFP
574 transgene in Nicotiana benthamiana is possibly mediated by small quantities of siRNA
575 that do not trigger systemic silencing. Plant J 45 (6):1006-1016. doi:10.1111/j.1365-
576 313X.2006.02664.x
577 Koscianska E, Kalantidis K, Wypijewski K, Sadowski J, Tabler M (2005) Analysis of RNA
578 silencing in agroinfiltrated leaves of Nicotiana benthamiana and Nicotiana tabacum.
579 Plant Mol Biol 59 (4):647-661. doi:10.1007/s11103-005-0668-x
580 Kumakura N, Takeda A, Fujioka Y, Motose H, Takano R, Watanabe Y (2009) SGS3 and
581 RDR6 interact and colocalize in cytoplasmic SGS3/RDR6-bodies. FEBS Lett 583
582 (8):1261-1266. doi:10.1016/j.febslet.2009.03.055
583 Liu L, Chen X (2016) RNA Quality Control as a Key to Suppressing RNA Silencing of
584 Endogenous Genes in Plants. Molecular plant 9 (6):826-836
585 Luo Z, Chen Z (2007) Improperly terminated, unpolyadenylated mRNA of sense transgenes is
586 targeted by RDR6-mediated RNA silencing in Arabidopsis. The Plant cell 19 (3):943-
587 958
588 Manavella PA, Koenig D, Weigel D (2012) Plant secondary siRNA production determined by
589 microRNA-duplex structure. Proc Natl Acad Sci U S A 109 (7):2461-2466.
590 doi:10.1073/pnas.1200169109
591 McHale M, Eamens AL, Finnegan EJ, Waterhouse PM (2013) A 22-nt artificial microRNA
592 mediates widespread RNA silencing in Arabidopsis. Plant J 76 (3):519-529.
593 doi:10.1111/tpj.12306
594 Milne I, Stephen G, Bayer M, Cock PJ, Pritchard L, Cardle L, Shaw P,Marshall D (2013)
595 Using Tablet for visual exploration of secondgeneration sequencing data. Brief
596 Bioinform 14:193–202.
597 Mlotshwa S, Pruss GJ, Peragine A, Endres MW, Li J, Chen X, Poethig RS, Bowman LH,
598 Vance V (2008) DICER-LIKE2 plays a primary role in transitive silencing of
599 transgenes in Arabidopsis. PloS one 3 (3):e1755
600 Moissiard G, Parizotto EA, Himber C, Voinnet O (2007) Transitivity in Arabidopsis can be
601 primed, requires the redundant action of the antiviral Dicer-like 4 and Dicer-like 2,
602 and is compromised by viral-encoded suppressor proteins. RNA (New York, NY 13
603 (8):1268-1278

604 Montgomery TA, Howell MD, Cuperus JT, Li D, Hansen JE, Alexander AL, Chapman EJ,
605 Fahlgren N, Allen E, Carrington JC (2008a) Specificity of ARGONAUTE7-miR390
606 interaction and dual functionality in TAS3 trans-acting siRNA formation. Cell 133
607 (1):128-141
608 Montgomery TA, Yoo SJ, Fahlgren N, Gilbert SD, Howell MD, Sullivan CM, Alexander A,
609 Nguyen G, Allen E, Ahn JH, Carrington JC (2008b) AGO1-miR173 complex initiates
610 phased siRNA formation in plants. Proceedings of the National Academy of Sciences
611 of the United States of America 105 (51):20055-20062
612 Parent JS, Jauvion V, Bouche N, Beclin C, Hachet M, Zytnicki M, Vaucheret H (2015) Post-
613 transcriptional gene silencing triggered by sense transgenes involves uncapped
614 antisense RNA and differs from silencing intentionally triggered by antisense
615 transgenes. Nucleic Acids Res 43 (17):8464-8475. doi:10.1093/nar/gkv753
616 Philips JG, Naim F, Lorenc MT, Dudley KJ, Hellens RP, Waterhouse PM (2017) The widely
617 used Nicotiana benthamiana 16c line has an unusual T-DNA integration pattern
618 including a transposon sequence. PLoS One. 23;12(2):e0171311. doi:
619 10.1371/journal.pone.0171311.
620 Pontes O, Vitins A, Ream TS, Hong E, Pikaard CS, Costa-Nunes P (2013) Intersection of
621 small RNA pathways in Arabidopsis thaliana sub-nuclear domains. PLoS One 8
622 (6):e65652. doi:10.1371/journal.pone.0065652
623 Sakurai Y, Baeg K, Lam AYW, Shoji K, Tomari Y, Iwakawa HO (2021). Cell-free
624 reconstitution reveals the molecular mechanisms for the initiation of secondary siRNA
625 biogenesis in plants. Proc Natl Acad Sci U S A 3;118(31)
626 Schiebel W, Haas B, Marinkovic S, Klanner A, Sanger HL (1993) RNA-directed RNA
627 polymerase from tomato leaves. II. Catalytic in vitro properties. The Journal of
628 biological chemistry 268 (16):11858-11867
629 Shi CY, Kingston, ER, Kleaveland, B, Lin DH, Stubna MW, Bartel, DP (2020) The ZSWIM8
630 ubiquitin ligase mediates target-directed microRNA degradation. *Science (New York,*
631 *N.Y.)*, *370*(6523), eabc9359
632 Tsuzuki M, Motomura K, Kumakura N, Takeda A (2017) Interconnections between mRNA
633 degradation and RDR-dependent siRNA production in mRNA turnover in plants. J
634 Plant Res 130 (2):211-226
635 Uslu VV, Bassler A, Krczal G, Wassenegger M (2020) High-Pressure-Sprayed Double
636 Stranded RNA Does Not Induce RNA Interference of a Reporter Gene. Front Plant Sci
637 11:534391. doi:10.3389/fpls.2020.534391
638 Vaistij FE, Jones L (2009) Compromised virus-induced gene silencing in RDR6-deficient
639 plants. Plant physiology 149 (3):1399-1407
640 Vaistij FE, Jones L, Baulcombe DC (2002) Spreading of RNA targeting and DNA
641 methylation in RNA silencing requires transcription of the target gene and a putative
642 RNA-dependent RNA polymerase. Plant Cell 14 (4):857-867. doi:10.1105/tpc.010480
643 Vermeersch L, De Winne N, Depicker A (2010) Introns reduce transitivity proportionally to
644 their length, suggesting that silencing spreads along the pre-mRNA. Plant J 64
645 (3):392-401
646 Vermeersch L, De Winne N, Nolf J, Bleys A, Kovarik A, Depicker A (2013) Transitive RNA
647 silencing signals induce cytosine methylation of a transgenic but not an endogenous
648 target. Plant J 74 (5):867-879
649 Voinnet O, Baulcombe DC (1997) Systemic signalling in gene silencing. Nature 389
650 (6651):553. doi:10.1038/39215
651 Wassenegger M, Heimes S, Riedel L, Sanger HL (1994) RNA-directed de novo methylation
652 of genomic sequences in plants. Cell 76 (3):567-576. doi:10.1016/0092-
653 8674(94)90119-8

654 Wassenegger M, Krczal G (2006) Nomenclature and functions of RNA-directed RNA
655 polymerases. Trends in plant science, 11(3), 142–151.
656 https://doi.org/10.1016/j.tplants.2006.01.003
657 Wu H, Li B, Iwakawa H, Pan Y, Tang X, Ling-hu Q, Liu Y, Sheng S, Feng L, Zhang H,
658 Zhang X, Tang Z, Xia X, Zhai J, Guo H (2020a) Plant 22-nt siRNAs mediate
659 translational repression and stress adaptation. Nature. doi:10.1038/s41586-020-2231-y
660 Yoshikawa M, Peragine A, Park MY, Poethig RS (2005) A pathway for the biogenesis of
661 trans-acting siRNAs in Arabidopsis. Genes & development 19 (18):2164-2175
662 Yu A, Saudemont B, Bouteiller N, Elvira-Matelot E, Lepère G, Parent JS, Morel JB, Cao J,
663 Elmayan T, Vaucheret H (2015) Second-Site Mutagenesis of a Hypomorphic
664 argonaute1 Allele Identifies SUPERKILLER3 as an Endogenous Suppressor of
665 Transgene Posttranscriptional Gene Silencing. Plant Physiol. 169(2):1266-74. doi:
666 10.1104/pp.15.00585.
667
668

669

670
671
672 **FIGURE LEGENDS**
673
674 **Figure 1| Local silencing phenotypes obtained by 22-nt siRNAs**. (a) 35S promoter (p35S),
675 Green Fluorescent Protein 5 coding region (GFP5) and NOPALINE SYNTHASE terminator
676 (tNOS) is shown. The exact location of where siRNA#164, siRNA#386, and siRNA739 map
677 on the GFP are provided as #164-188, #386-410, #739-763, respectively. The RNA duplex
678 sequences of the siRNAs with 3' 2 nt overhangs are provided and U-A base pairing at the 5'
679 ends are shown in red letters. (b) Local silencing at 6 dps were documented for the whole
680 plant and single leaves under the UV light. Fully GFP expressing plants have green stems,
681 orange leaves. The silenced areas appear in red. The numbers on the left panel indicate the
682 number of plants showing local silencing and the total number of plants used for the treatment.
683 The red silenced areas on the right panel were excised and used for sRNA-seq. (c) Systemic
684 silencing at 35 dps were documented on the whole plant under UV light and single leaves
685 under GFP and Far Red fluorescence using PharosFX Imager. The silenced areas appear in
686 red. The numbers on the left panel indicate the number of plants showing systemic silencing
687 and the total number of plants used for the treatment.
688
689 **Figure 2| Silencing phenotypes obtained by 21-nt siRNAs**. (a) 35S promoter (p35S), Green
690 Fluorescent Protein 5 coding region (GFP5) and NOPALINE SYNTHASE terminator (tNOS)
691 is shown. The exact location of where siRNA#164-21nt, siRNA#739-21nt map on the GFP
692 are provided as #165-188 #740-763, respectively. The RNA duplex sequences of the siRNAs
693 with 3' 2 nt overhangs are provided and U-A base pairing at the 5' ends are shown in red
694 letters. (b) The upper panel shows the whole plants sprayed with the corresponding siRNAs,
695 imaged under the UV light. Fully GFP expressing plants have green stems, orange/green
696 leaves. The silenced areas appear in red (shown with white arrows). The lower panel shows
697 composite images of the silenced leaves under GFP and Far Red fluorescence using PharosFX
698 Imager. (c) The red silenced areas compared to the whole leaf were calculated. The composite
699 images in the the lower panel were used for quantification by FIJI for three leaves each
700 treatment. The error bars indicate standard error. No significant (ns) differences in silent areas
701 found.
702

703 **Figure3| Quantity and quantitative distribution of transitive siRNAs along GFP.** (a) The
704 graph shows normalized read counts of 21-, 22- and 24-nt combined along GFP. Each of 21-,
705 22-, and 24-nt reads mapping to the GFP is normalized to total 21-, 22-, and 24-nt reads in the
706 sample and multiplied with 10^6 for each position along the GFP. These normalized values of
707 21-, 22- and 24-nt siRNAs are summed up for each biological replicate and the average value
708 of the biological replicates are shown in a sliding window of 10 nt. In the X-axis, the
709 translational start site, the stop codon and the position, where the siRNAs map are provided
710 together with Transitivity Hot Spot (THS). (b) Percent density distribution (pdd) is calculated
711 for each position (see Materials and Methods). The average pdd values of biological replicates
712 are plotted in a sliding window of 10 nt and the percentage values for each position is given in
713 Y-axis. The relevant positions along the GFP are given in X-axis. (c) The normalized counts
714 of combined 21-, 22-, and 24-nt long reads mapping to GFP are plotted for each siRNA
715 treatment. The values of each biological replicate are shown as data points in the bar chart.
716 Student's t-test is used for pairwise comparison (***, $p<10^{-3}$). (d) The distance between the
717 peaks, shared among all three siRNA treatments are calculated and provided in a bar chart.
718 Horizontal axis shows the distance in the unit of base pairs. In all the charts and graphs,
719 siRNA#164 is shown in blue, siRNA#386 in orange, and siRNA#739 is grey.
720
721 **Figure 4| Regional and strand-specific distribution of transitive siRNAs.** (a) Regional
722 percent distribution of 21-, 22- and 24-nt reads (rpd-sRNA, see Materials and Methods)
723 between the positions given in the X-Axis in addition to THS, which is taken as a separate
724 area. For each treatment, the average rpd-sRNA of three biological replicates are plotted. The
725 error bars indicate standard deviation and student's t-test is used for pairwise statistical
726 comparison between different siRNA treatments. (b) In order to avoid size-bias in rpd-sRNA,
727 average percent read density per base pair (ARDPB, see Materials and Methods) is plotted to
728 compare the rpd-sRNA between different regions for each siRNA treatment. The ARDPB
729 decreases as the region is further away from THS for all siRNA treatments. The position of
730 the siRNAs used for the experiment is shown in the X-axis with respect to the six regions of
731 interest. (c) Strand specific ARDPB is plotted for the regions given in the X-axis. Y axis
732 shows the ARDPB in terms of percent probability for sense (bars with solid colours above the
733 X-axis, and bars with diagonal patterns below the X-axis). Student t-test is used for pairwise
734 comparisons between siRNA treatments in the given region. In all the charts siRNA#164 is
735 shown in blue, siRNA#386 in orange, and siRNA#739 in grey.
736
737 **Figure 5| Comparison of 21-, 22- and 24-nt transitive siRNAs.** (a) Average of total 21-, 22-,
738 and 24-nt reads mapping to GFP normalized to 21-nt reads mapping to GFP of three
739 biological replicates upon siRNA treatments. Regardless of the siRNA treatment, 22-nt reads
740 are one third of the 21-nt reads and 24-nt reads are one seventh of the 21-nt reads on both
741 sense (solid colours above X-axis) and anti-sense strand (diagonal pattern below X-axis). (b)
742 The ratio of 21-, 22- and 24-nt reads mapping to GFP regardless of the strand, normalized to
743 the total number of sRNAs of 21-, 22- and 24-nt siRNA reads, respectively, for each position
744 on GFP. The value is multiplied with 10^6 and the graph is plotted in a sliding window of 10 nt.
745 siRNA#164 treatment is shown in blue, siRNA#386 in orange, and siRNA739 in grey. From
746 the darkest to the lightest tone of each colour, 21-, 22-, and 24-nt long reads are plotted,
747 respectively.
748
749 **Figure 6| Strand Specific Distribution of 21- and 22-nt transitive siRNAs.** (a) The ratio of
750 21- siRNA reads mapping to GFP, normalized to the total number of sRNAs of 21- reads for
751 each position on GFP (b). The ratio of 22- siRNA reads mapping to GFP, normalized to the
752 total number of sRNAs of 22- reads for each position on GFP. The values are multiplied with
753 10^6 and the graph is plotted in a sliding window of 10 nt in a strand specific manner (See

754 Materials and Methods). Sense strand is plotted with a solid line above the X-axis with and
755 anti-sense strand is plotted with a dotted line below the X-axis. Black arrows show the THS
756 peak, which is more prominent on the sense strand, whereas purple arrow depicts a 22-nt
757 siRNA read peak in the sense strand, which is lacking in the anti-sense strand.
758
759 **Figure 7| A model for the role of siRNAs in transitivity.** A plant gene may generate either
760 legitimate mRNAs or aberrant RNAs (abRNAs) that lack a 5' cap structure and/or a 3'
761 polyadenylation tail. In the absence of siRNAs, abRNAs above a certain threshold, posing a
762 potential deleterious effect on the plant cell, are channeled (primarily) to RDR6-mediated
763 decay (sense PTGS) (top left panel) and (secondarily) to competing exonucleolytic RNA
764 decay pathways (not shown). In the presence of 21-nt siRNAs, abRNAs are targeted and
765 cleaved by 21-nt siRNAs at the target site, with a comparable efficiency between 5' and 3'
766 target site (PTGS) (top right panel). The cleavage products are not processed, at least
767 significantly, by RDR6, but are rapidly degraded by exonucleolytic pathways (as typically
768 happens in the case of 21-nt miRNA cleavage products) (not shown). In the presence of 22-nt
769 siRNAs, AGO1 conformation is seemingly affected by 22-nt siRNA loading (or by small
770 RNAs containing an asymmetric bulge) and this impairs AGO/RISC capacity for cleavage.
771 Instead, AGO1-loaded 22-nt siRNAs, targeting 5' of the target efficiently recruit RDR6 to the
772 3' end of abRNAs, possibly with a mediator such as SDE3, SDE5, and SGS3 (bottom left
773 panel). On the other hand, AGO1-loaded 22-nt siRNAs, targeting 5' of the target create a
774 steric hindrance for RDR6 recruitment and reduce RNA dependent RNA polymerase (RdRp)
775 activity (bottom right panel). RDR6 can move along a distance of approximately 700 nt,
776 generating 21-nt secondary siRNAs (transitivity). The resulting dsRNA is cleaved
777 hierarchically by DCL4, DCL2, and in negligible amounts by DCL3. These secondary 21-nt
778 siRNAs cleave homologous mRNAs and abRNAs (local PTGS) and can be transported
779 through the plasmodesmata to neighboring cells. Importantly, during the process of
780 transitivity, an RNA signal of yet unidentified nature is generated and transported through the
781 phloem to establish systemic PTGS to distant parts of the plant. In this model RDR6 is shown
782 to process only abRNA and not mRNAs. Indeed, polyadenylation tails were shown to inhibit
783 RDR6 transcription, a meaningful evolutionary strategy to avoid generation of U-only
784 siRNAs which could indiscriminately target any given mRNA for PTGS.
785
786
787
788
789
790
791
792
793
794
795
796
797
798
799
800
801
802
803
804

805 **FIGURES**

806 **Figure 1:**

807

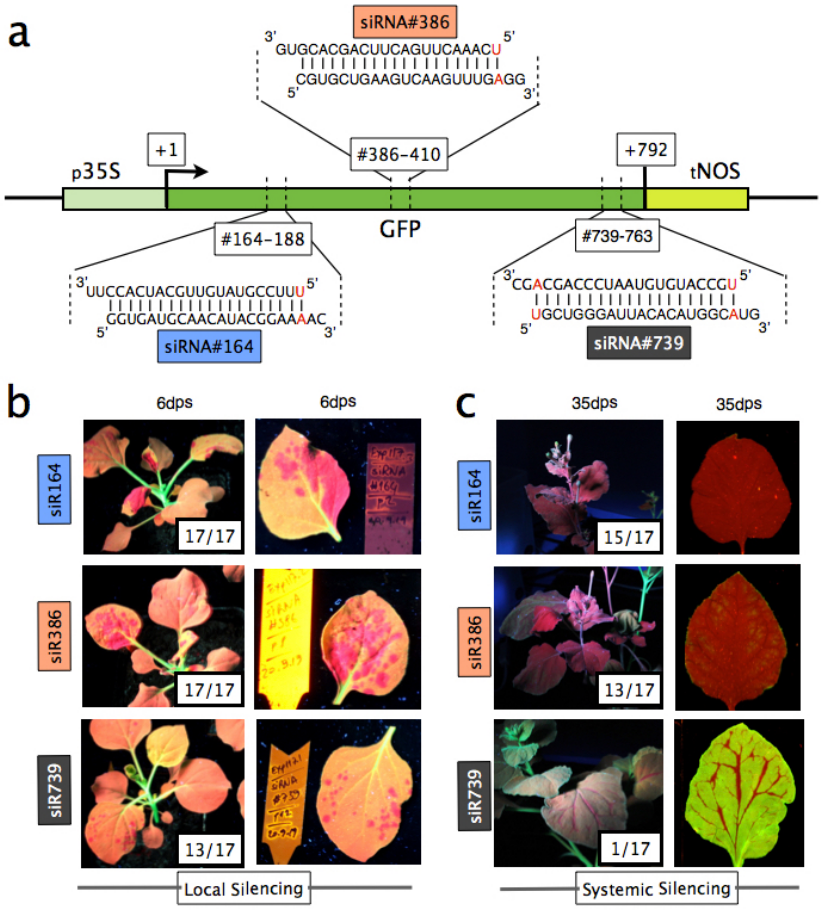

808

809

810 **Figure 2:**

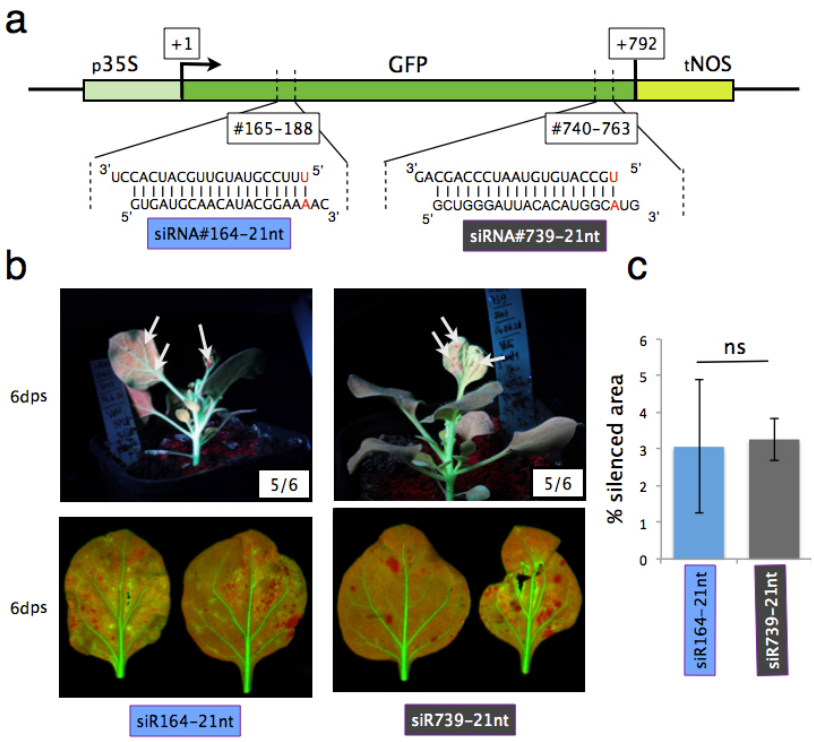

811

Figure3

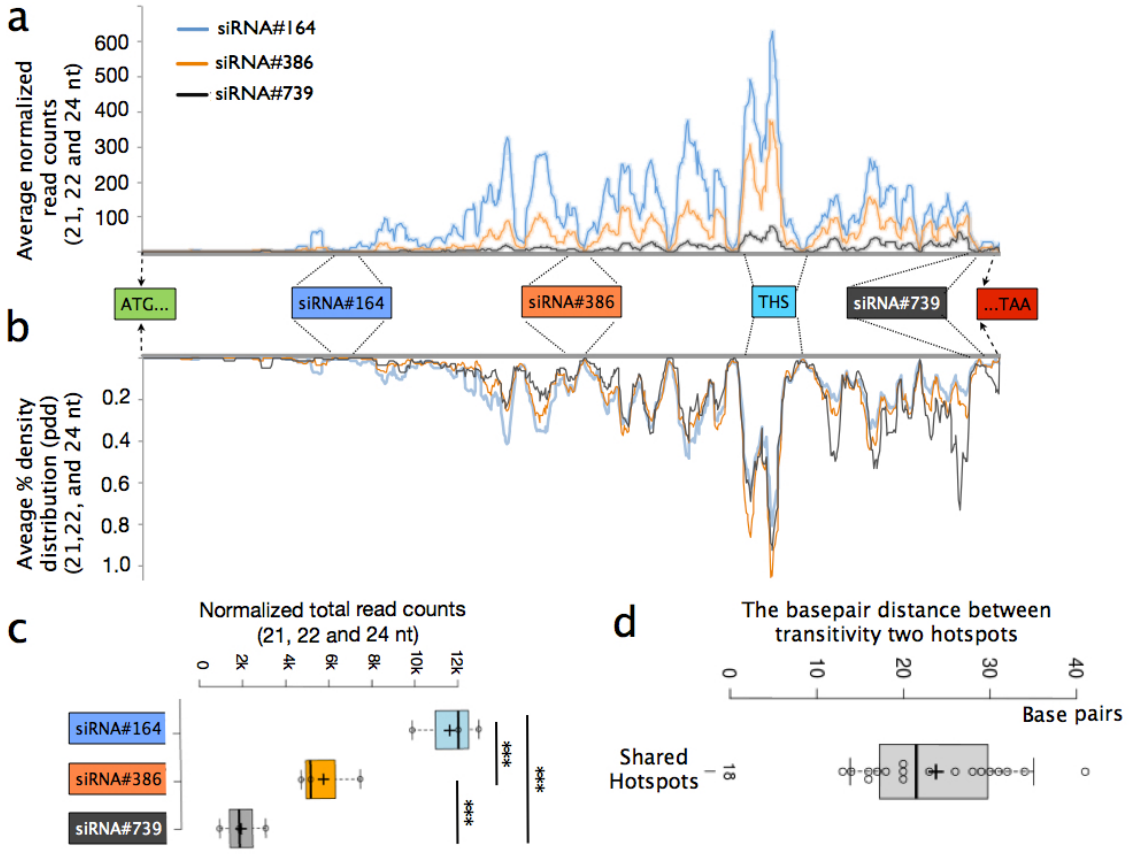

Figure4

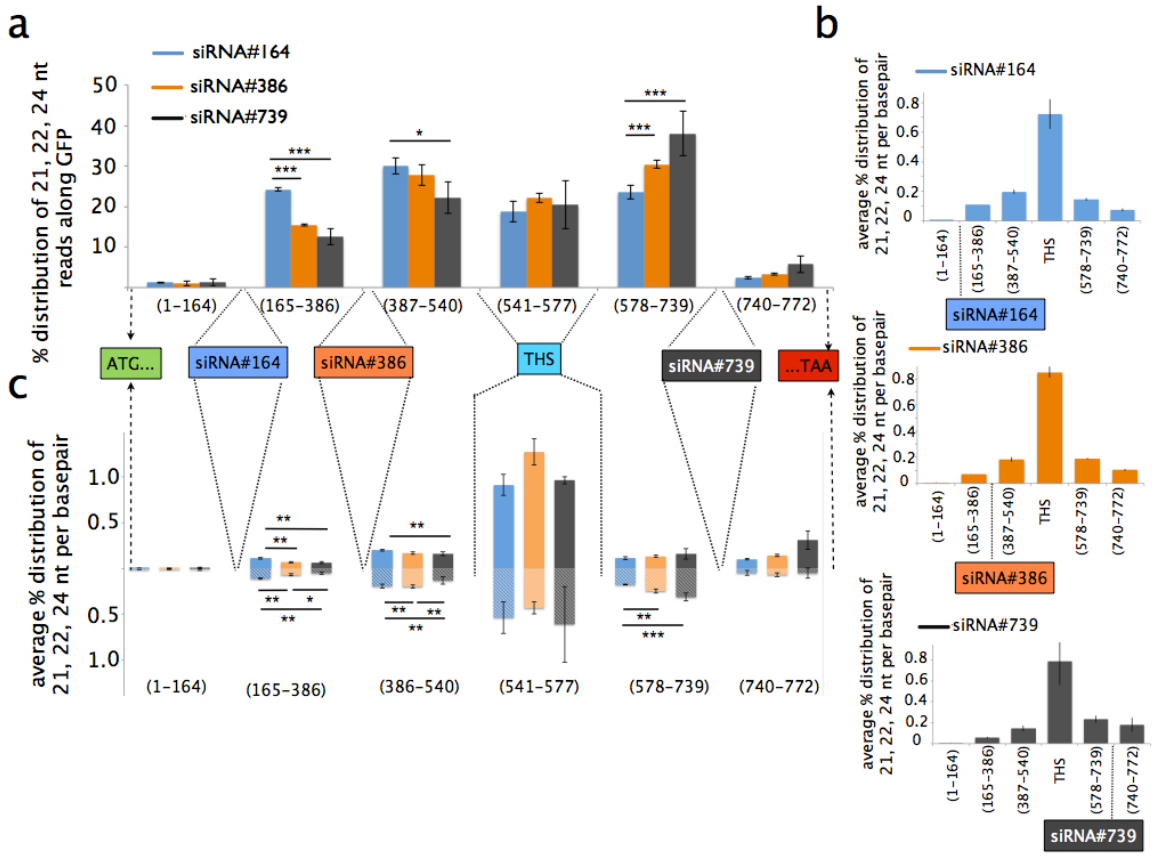

817 **Figure 5:**

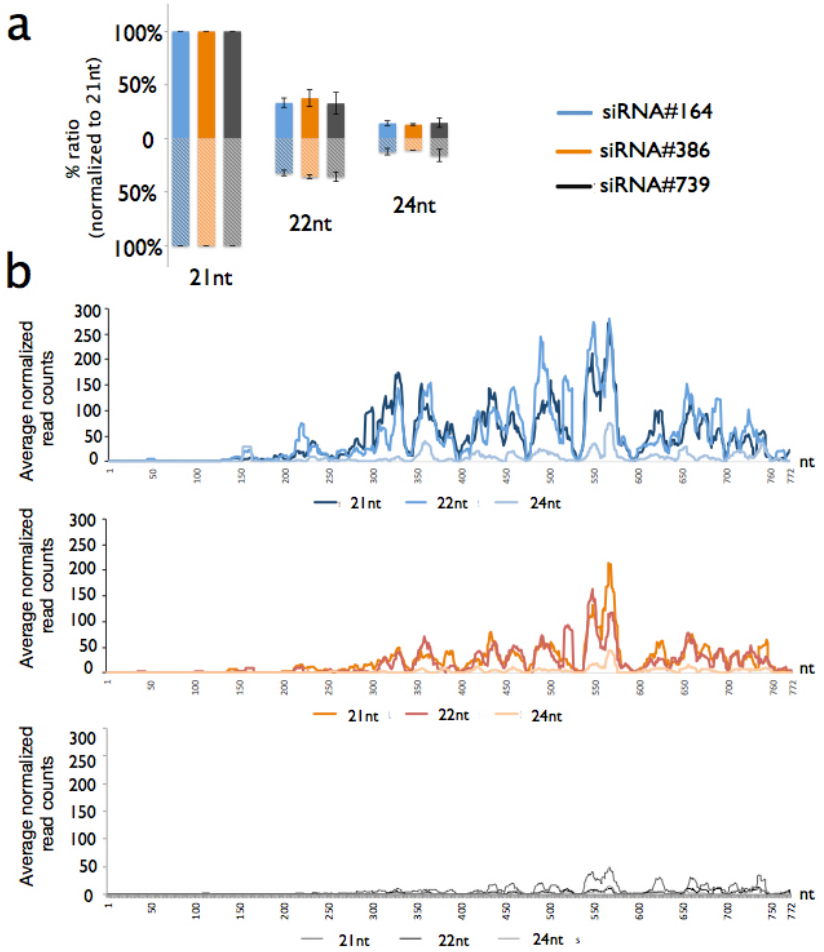

818
819
820 **Figure 6:**
821

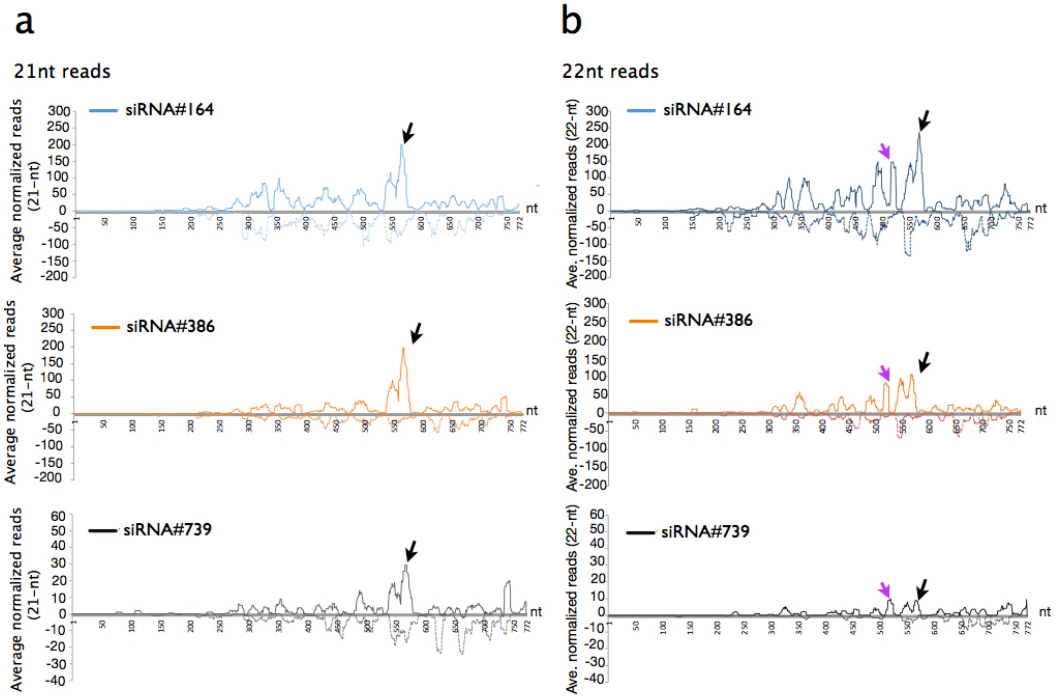

822

823 **Figure7:**
824

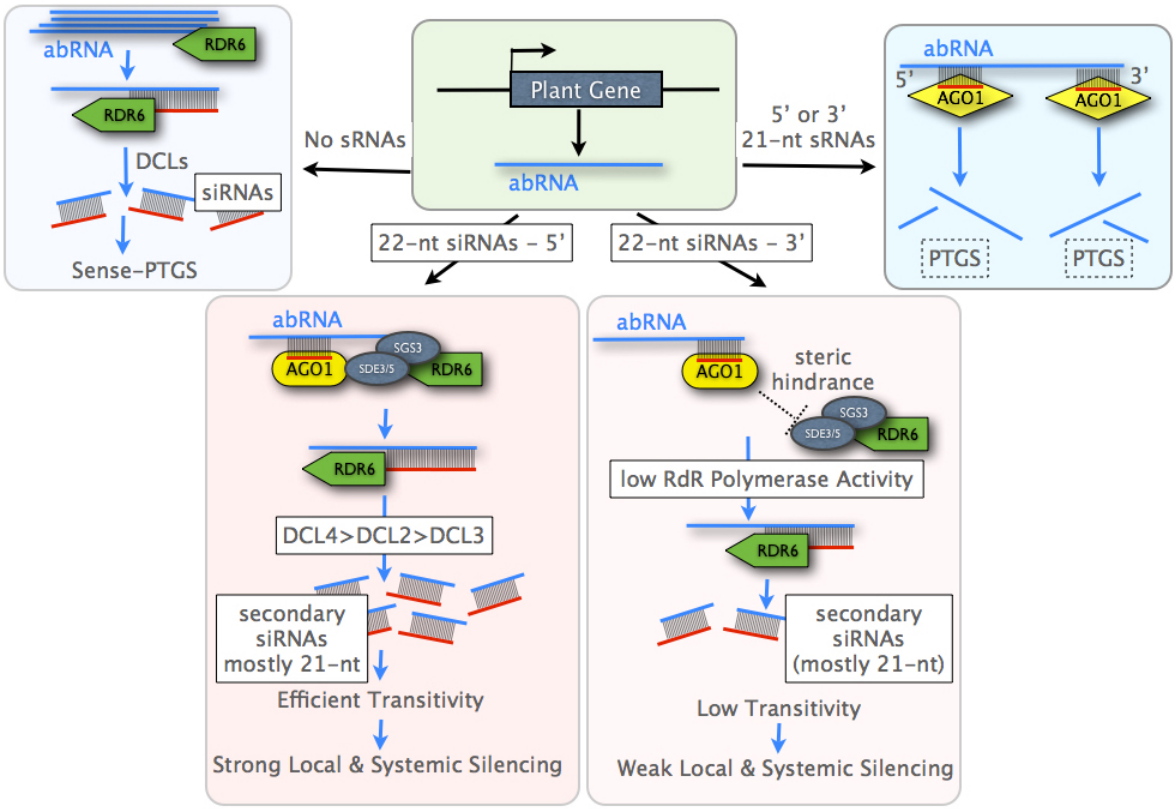

825
826 **Figure S1:**
827

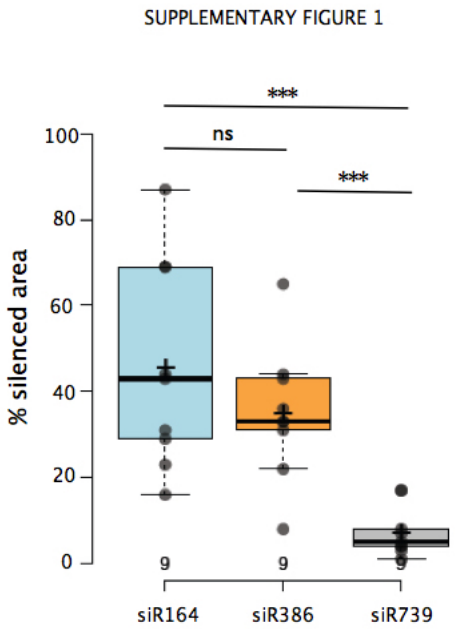

828
829
830
831
832
833

834
835 **Figure S2:**
836

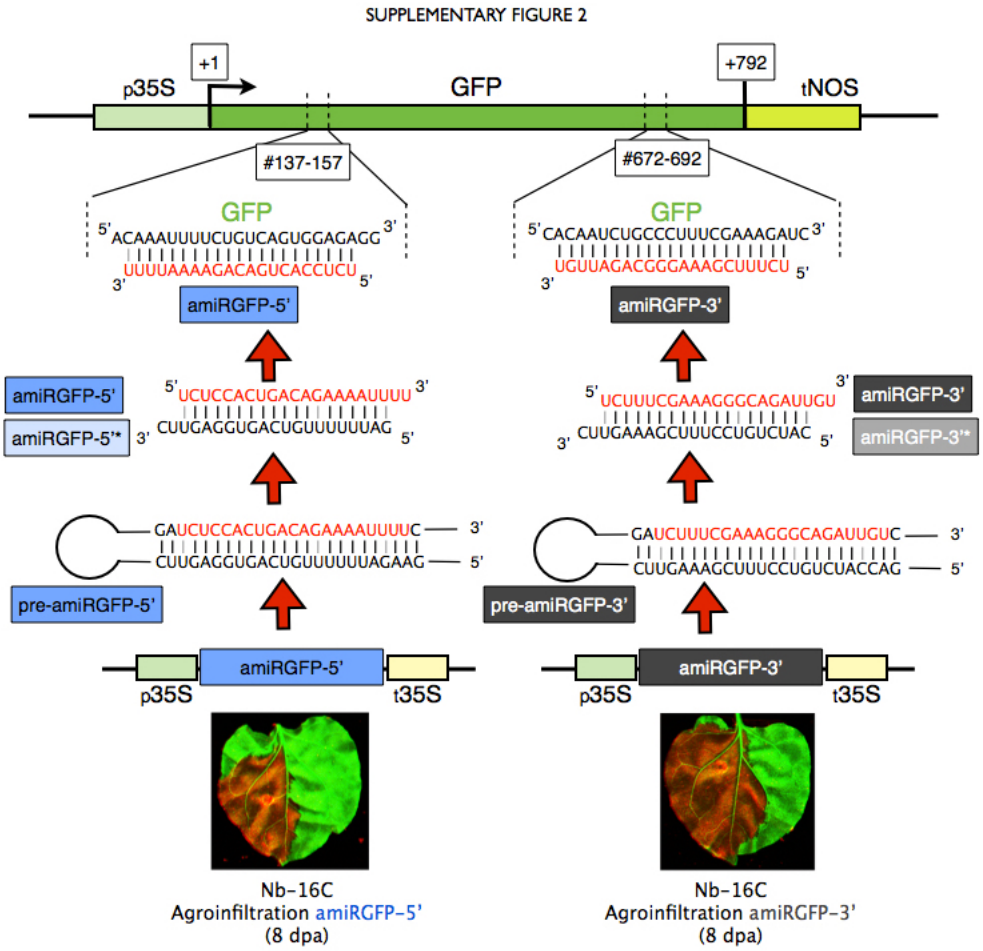

837
838 **Figure S3:**
839

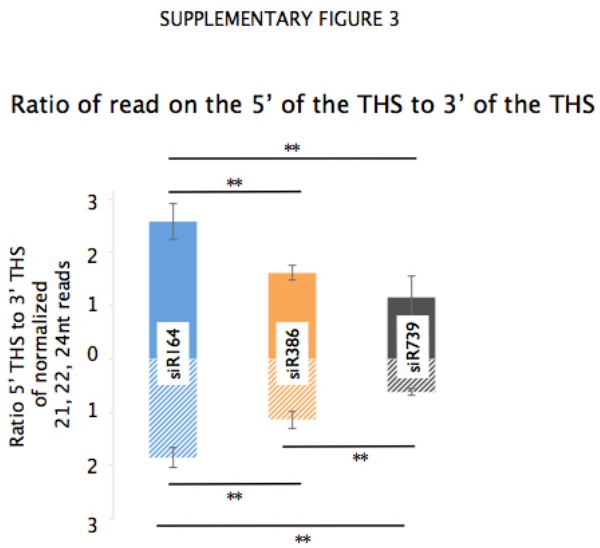

840
841
842
843

844 **Supplementary Table 1**

845

	total reads	21nt	22nt	24nt		22nt-All	22nt reads mapping to sprayed siRNAs
164_1	4369898	172793	69028	159097		113124	44096
164_2	3730724	163838	31004	103126		185600	154596
164_3	2960764	101214	32222	74411		99776	67554
386_4	3280249	98369	47037	89837		64847	17810
386_5	2845604	133271	61026	109896		91443	30417
386_6	3093553	81749	29355	66598		59341	29986
739_7	3494055	132018	39471	118383		138770	99299
739_8	3149294	85241	27560	50388		95000	67440
739_9	3215061	93197	27114	56642		103919	76805

846